JOURNAL OF MATERIALS SCIENCE 28 (1993) 5019–5031

Formation of solid particles by hydrolysis of cerium (IV) sulphate

Part I *Time evolution of the hydrolysed solutions*

V. BRIOIS, C. E. WILLIAMS, H. DEXPERT, F. VILLAIN
LURE, Université Paris-Sud, 91405 Orsay Cedex, France

B. CABANE
DSPC, CEN-Saclay, 91191 Gif-sur-Yvette Cedex, France

F.DENEUVE, C. MAGNIER
Rhône-Poulenc, CRA, 52 rue de la Haie Coq, 93308 Aubervilliers Cedex, France

Uniform particles of controlled morphology of $CeOSO_4 \cdot H_2O$ may be prepared by forced hydrolysis, at 90 °C, of solutions of cerium (IV) sulphate. A structural description is given here of the different steps of the forced hydrolysis before precipitation takes place. It uses essentially the complementary techniques of extended X-ray absorption fine structure spectroscopy and small-angle X-ray scattering to characterize, at different length scales, the structural evolution of the solution. The first step, which occurs as temperature is raised above 60 °C, is an inorganic polymerization that transforms molecular dimeric precursors $Ce_2(OH)_2O_{12}$ into colloidal particles. In the second step, at the ageing temperature of 90 °C, no chemical and structural changes are revealed; the solution has reached an equilibrium state characterized by the presence of 3 nm large monodisperse colloids which use 85% of the initial cerium ions and smaller particles (15%). The detailed local structure around the cerium atoms in the colloids is compatible with the formation of a chain-like structure of Ce(IV) ions via hydroxo bridges $(Ce(OH)_2)_n^{2n+}$. A mechanism to explain the transformation of precursors into colloids is proposed.

1. Introduction

Control of the morphology of the elementary building blocks is a prerequisite for producing high-performance materials such as ceramics, catalysts, coatings, etc. [1–3]. In this respect, much research, both in industrial and academic circles, has been devoted to the production of monodisperse particles with a well-defined geometry [4–13]. These particles can be produced by precipitation from homogeneous solution containing various molecular precursors. A precise control of each step of the complex reactions leading from precursors to solid particles is essential to obtain "tailored" building blocks.

Amongst the possible techniques, thermohydrolysis of metal salts in an acid medium has been one of the favourite ones because it is simple to use, it is applicable to numerous metal salts and it produces particles with a great variety of shapes (sphere, cube, rod, disc, etc.) and sizes (nanometric to micrometric size) [14–27]. Although the importance of parameters such as temperature, pH, salt concentration, anion type, has been well recognized, it is still impossible to predict the outcome of a given thermohydrolysis.

We report here a chemical and structural characterization of the different steps during thermohydrolysis of cerium (IV) sulphate. Hsu *et al.* [25] have previously described the experimental conditions leading to the precipitation of cerium (IV) particles of various morphologies. Amongst these we have characterized each step in the formation of monodisperse solid particles of cerium (IV) oxysulphate from precursor to colloid. The process can be described according to a scheme presented in Fig. 1.

This paper describes the solution and sol states, their evolution from precursors to colloids before precipitation takes place. The time evolution of the forced hydrolysis (Steps I and II in Fig. 1) will be presented first. Because no significantly structural and/or chemical changes will be found to occur during Step II, a definite moment in the ageing of solutions at 90 °C will then be characterized in more detail. Finally, in the light of this characterization, possible structures for the precursors and colloids will be proposed.

The mechanism to explain the transformation of molecular precursors into colloidal particles and the characterization of the colloidal and final particles extracted from the solution will be left to two forthcoming papers (Parts II [28] and III [29], respectively, of this series).

2. Experimental procedure

2.1. Materials

The operative procedure we have used to obtain solid

0022–2461

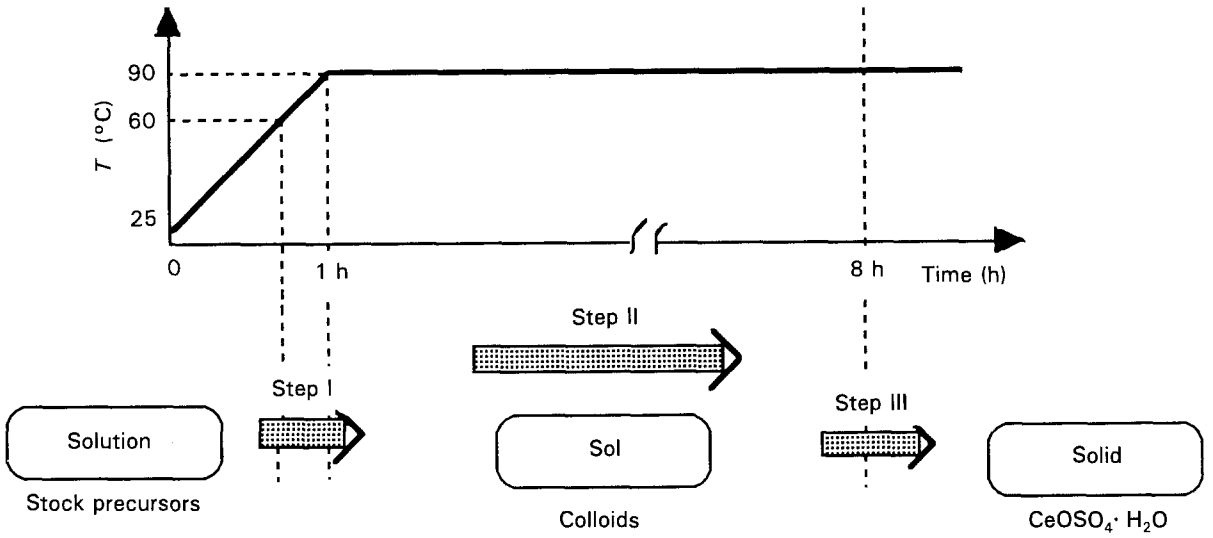

Figure 1 Apparition of three states during hydrolysis.

particles of cerium (IV) oxysulphate ($CeOSO_4 \cdot H_2O$) by forced hydrolysis of solutions of cerium (IV) sulphate in sulphuric acid has been inspired by that described by Hsu *et al.* [25] and only the relevant points will be presented here. For this investigation, all starting solutions are 10^{-1} M in $Ce(SO_4)_2 \cdot 4H_2O$ (Prolabo batch 88028) and 0.25 M in H_2SO_4 (concentrated sulphuric acid, Prolabo). The freshly prepared stock solution is filtered through a glass-fibre membrane (Prolabo) to eliminate possible particle contaminants or insoluble ceric salts. The heating is then carried out in a reactor with a double inner side where water thermalized at 90 °C circulates. Starting at room temperature, the ageing temperature is slowly reached (30 min to 1 h) and then the solution is maintained at 90 °C. Throughout the thermal treatment, the solution is constantly stirred by a magnetic rod. After 7–8 h, the solution becomes turbid and solid particles precipitate in the reactor. Contrary to Hsu's procedure [25] which leads to unidentified cylindrical solid particles of unidentified composition, the particles here prepared are of relatively spherical shape with internal substructure. The characterization and identification of the final particles are given in Part III [29]. Because the complete process is entirely reproducible, one can assume that the difference in morphology is due to differences between the two procedures.

Indeed, because the reproducibility of the forced hydrolysis is very sensitive to many parameters such as temperature, pH, ionic strength, as well as to the characteristics of the starting reagents, great care was taken to use the same experimental protocol for each hydrolysis. More specifically, we have used Ce(IV) salts from the same batch because it was found that the amount of adsorbed H_2SO_4 may vary and consequently the working conditions in Hsu's diagram [25].

In order to describe the system at different stages during the forced hydrolysis process, and before the precipitation of macroscopic solid particles, a small amount of solution is extracted from the reactor at regular time intervals and characterized by the various techniques described later. Because the Ce(IV) ion is a very strong oxidizing agent ($E°$/Ce(IV)/Ce(III) = 1.44 V, in H_2SO_4 0.5 M medium [30, 31]), and to avoid partial reduction of Ce(IV) in Ce(III), inert material such as teflon, kapton or carbon has been used exclusively for all equipment in contact with the Ce(IV) solutions, i.e. characterization containers, syringes, etc.

2.2. Experimental techniques

Because of the complexity of the system, different techniques have been used in parallel to monitor the appearance of particles in the thermohydrolysed solution, to determine their size, shape and local structure around the cerium atom and to follow their time evolution.

2.2.1 Small-angle X-ray scattering (SAXS)

Typically SAXS provides structural information in the 0.5–100 nm length range. Experiments were carried out using the small-angle scattering spectrometer D22 at the LURE-DCI synchrotron radiation source (Orsay, France) [32]. The fixed-exit double crystal monochromator was tuned to provide, at the sample, a 1 mm^2 beam of an energy of 9500 eV or a wavelength, λ, of 0.13 nm. The scattered intensity is recorded with a one-dimensional, gas-filled, position sensitive detector. Both X-ray energy and sample-to-detector distance can be adjusted to cover the desired range of scattering vector q, where $q = 4\pi \sin \theta/\lambda$; θ is one-half the scattering angle. Here SAXS data, obtained between $q = 0.18$ and 4.6 nm^{-1}, are plotted as the relative intensity versus q after correction for beam decay and sample absorption, and subtraction of the background scattering of a 0.25 M solution of H_2SO_4. Standard data analysis pertaining to solutions of non-interacting scattering particles have been used throughout. The size of these is obtained, using Guinier's law [33]: $I = I_0 \exp(-q^2 R_G^2/3)$ in the range $qR_G < 1$, where R_G is the radius of gyration. For spherical particles, the radius R_0 is related to R_G by $R_0 \approx 1.291\ R_G$.

Alternatively, the size may be obtained from the typical oscillations which appear in the scattering profile at larger angles; for monodisperse spherical particles, the first minimum occurs at $qR \approx 4.5$. A smoothing of the oscillations is due to a distribution in the sphere sizes and/or to a deviation from spherical shape [34].

Further information can be gained from the measurement of the invariant Q, defined as

$$Q = \int_0^\infty I(q)q^2 \, dq \quad (1)$$

For systems of isolated scatterers, it is proportional to the total volume V of the particles in the irradiated sample and to the mean square fluctuation of the electron density $(\Delta\rho)^2$ [35]

$$Q = 2\pi^2(\Delta\rho)^2 V \quad (2)$$

2.2.2. Extended X-ray absorption fine structure (EXAFS)

EXAFS is a powerful technique to obtain structural data on the local order in the 0.1–0.5 nm length range, information which are very useful in our case to combine with those coming from SAXS. Experiments were carried out using the EXAFS III or EXAFS IV spectrometers at the LURE-DCI storage ring (Orsay, France) running at 1.85 GeV. EXAFS data at the L_{III} edge of cerium (5723 eV) have been collected at room temperature using a double crystal monochromator (Si 1 1 1) with fixed exit geometry. Helium–neon (≈ 0.1 atm) and air (atmospheric pressure) filled ionization chambers were used to measure the flux intensity before and after sample, respectively. Third-order harmonics rejection was performed on the EXAFS III spectrometer by slightly detuning the parallelism of the crystals with a 30% incident photon flux loss and on the EXAFS IV spectrometer by using two parallel mirrors adjusted to suppress incident photons of energy higher than 8000 eV [36].

The EXAFS spectra were recorded within a 550 eV energy range, on the EXAFS III spectrometer in fast-running mode [37, 38], with a rate corresponding to 2 min for a scan, and on the EXAFS IV spectrometer with 1 eV steps, and 1 s accumulation time per point.

Measurements on solutions were made using a teflon cell possessing two kapton windows and an adjustable thickness in order to monitor sample absorbance.

The EXAFS analyses were processed using the classical plane-wave single scattering approximation, where the EXAFS signal $\chi(k)$ is expressed as a function of the wave-vector k of the photoelectron ejected from the absorbing atom by a sum of damped sine waves [39–43]

$$\chi(k) = \sum_j \left[N_j A_j(k) \exp(-2\sigma_j^2 k^2) \times \exp\left(\frac{-2R_j}{\lambda(k)}\right) \frac{\sin(2kR_j + \phi_{ij}(k))}{kR_j^2} \right] \quad (3)$$

where N_j is the number of atoms in the jth scattering shell at a distance R_j from the absorbing atom i, σ_j is the Debye–Waller factor; $\lambda(k)$ is the electron mean free path, $A_j(k)$ is the amplitude function relative to the jth shell, and $\phi_{ij}(k)$ the phase shift relative to the absorbing i and neighbour j pair. We used amplitude and phase functions tabulated by Mc Kale [44]. We checked that these tabulated values were correct for the standards CeO_2 and $Ce(SO_4)_2 \cdot 4H_2O$.

All the EXAFS data were treated according to the same procedure: after subtraction of the background, the normalized EXAFS signal $\chi(E) = [\mu(E) - \mu_0(E)]/[\mu_0(E)]$ (where $\mu_0(E)$ is the atomic-like absorption) was then transformed in k-space. The weighted $k^3\chi(k)$ EXAFS signal is then Fourier transformed to R distance space, using the same Hanning window function over 330 eV. The contributions of the neighbouring shells are filtered in R space. Then the structural parameters N_j, R_j and σ_j are extracted using a least-square fitting procedure. For the fit, a variation ΔE_0 is introduced to take into account any approximation in the determination of the absorption edge, E_0.

2.2.3. 1H NMR and pH measurements

Classical pH-metric methods are not available in this system, because the strong oxidizing power of cerium (IV) ions disturbs the pH measurements. Therefore, the proton concentration has been deduced from ^{1}H NMR measurements [45]. The latter are made using a Bruker MSL300 spectrometer at 298 K controlled temperature. The H^+ concentration is determined from the $\delta(^1H)$ chemical shift of the peak related to free protons in exchange with protons of solvent. A linear relation between the H^+ concentration and the $\delta(^1H)$ chemical shift of this peak is obtained after calibration in 0.2 M Na_2SO_4 solution at six different concentrations in sulphuric acid.

2.2.4. Ultracentrifuge and density measurements

Ultracentrifuge analysis allows us to deduce the size and the molecular weight from measurement of the sedimentation coefficient of the particles in solution [46]. These have been obtained with a Beckmann Spinco model E Ultracentrifuge using schlieren optics, i.e. by measuring the gradient of refractive index along the cell. The ultracentrifugation has been performed either at 44 000 r.p.m. for 1 h for the study of the sedimentation, or at 50 000 r.p.m. for 15 h for a preparative centrifugation.

For isolated spherical particles, the sedimentation coefficient, S_0, extrapolated at zero concentration, is related to the molar weight of the particle, M, by [47, 48]

$$S_0 = (1 - \rho_0 V_{ps}) \frac{M}{\mathcal{N} 6\pi\eta R} \quad (4)$$

where $\mathcal{N}$ is Avogadro's number, V_{ps} is the partial specific volume of the particle, ρ_0 is the solution density, and η is the absolute viscosity of the solvent.

It is possible to extrapolate from the sedimentation coefficient distribution, the molar weight, M_{cp}, and the radius R_{cp}, of the spherical particles. The parameters V_{ps} and ρ_0 are determined independently.

No correction was applied to the experimental S coefficient sedimentation for diffusion effects or concentration effects. The S_0 sedimentation coefficient is the experimental value determined for solutions 0.1 M in cerium (IV).

2.2.5. Transmission electron microscopy (TEM)

High-resolution imaging and analysis has been performed on a Philips CM30 (300 kV) transmission electron microscope (TEM).

3. Results

3.1. Macroscopic description

From a macroscopic point of view, the forced hydrolysis is characterized by a slight colour change of the transparent solution between room temperature, where it is golden yellow, and 90 °C, before precipitation, where it has a rather lemon colour. This colour difference can be explained by an increase of the pH of the solutions as thermohydrolysis proceeds. Indeed a shift of the ultraviolet absorption band (in the range 300–320 μm) has been found in an investigation of sulphato complexes of cerium (IV) when the H_2SO_4 concentration increases [49–51]. When precipitation occurs after 7–8 h thermal treatment, the solution in the reactor becomes increasingly turbid.

3.2. Time evolution of the forced hydrolysis

3.2.1. Size determination

Fig. 2 shows the evolution of the SAXS profiles of the solution, $I(q)$ versus q, between room temperature (≈ 25 °C) and the ageing temperature ($T = 90$ °C). Three regimes can be seen. In Regime I, up to 50 °C, the solution does not scatter in the SAXS range indicating that there are no species larger than about 0.5 nm in the stock solution. Above 60 °C, the intensity increases with temperature as scatterers appear in solution. This is Regime II. In Regime III, when the ageing temperature is reached, oscillations appear in the profile, better seen in a logarithmic representation $\ln I(q)$ versus $\ln q$ (Fig. 3). Then, as time passes and the solution ages for a few hours, the profile does not change: the 75 and 490 min curves are identical.

As opposed to Regime I where the solution contains what we can call "precursors' and no larger oligomeric species, Regime II is characterized by the appearance of "colloids", whose radius of gyration, R_G, measured by Guinier's law [24], increases from 0.49 nm to 1.23 nm. The estimated error is about 10%. Their radius, R_0, assuming spherical colloids, is plotted in Fig. 4 as a function of time. In Regime III, the oscillations are characteristic of the form factor of an assembly of fairly monodisperse spheres (or ellipsoids). The radius is estimated to be 1.8 nm from the

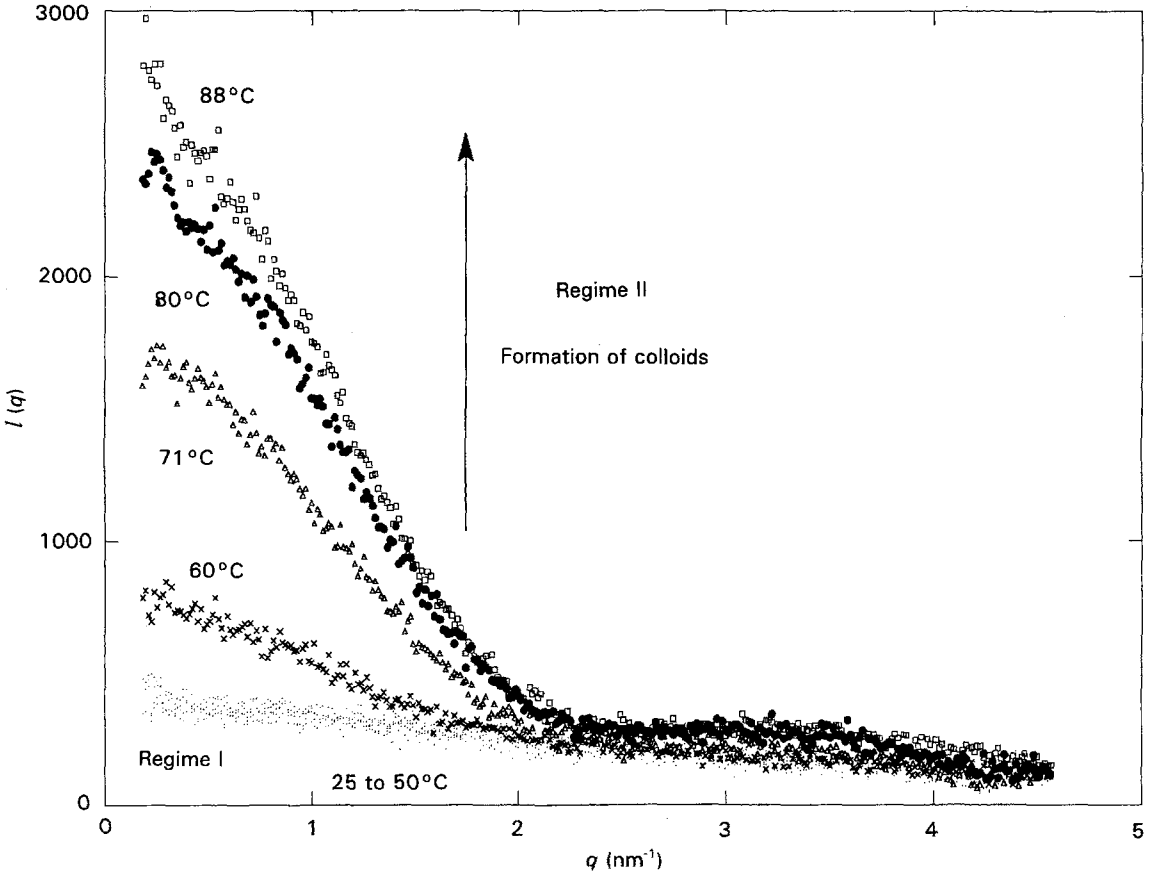

Figure 2 Evolution of the SAXS profiles of the solution, $I(q)$ versus q, between room temperature and ageing temperature, during the first hour of hydrolysis.

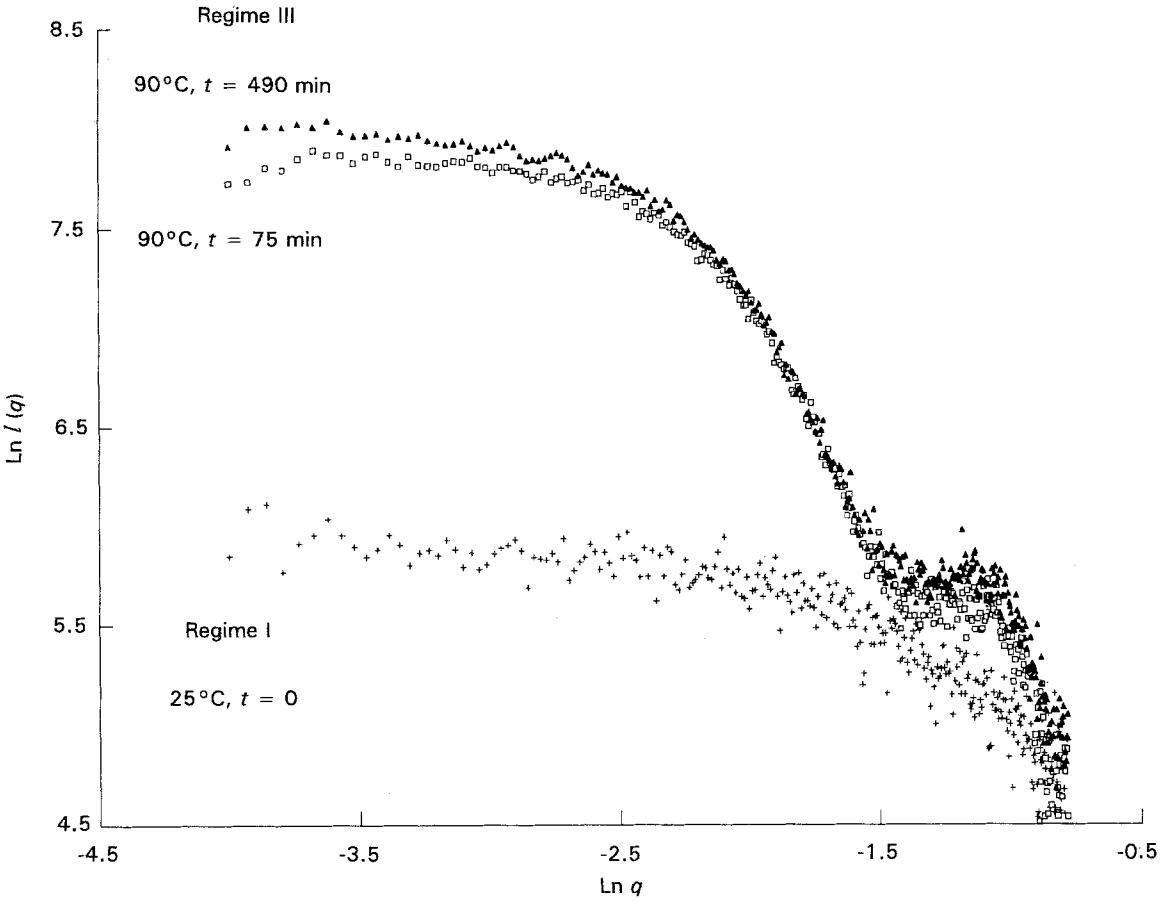

Figure 3 Logarithmic representation of the SAXS profiles of solutions, ln $I(q)$ versus ln q, when the ageing temperature is reached (90 °C) at 75 and 490 min hydrolysis, compared to the one of the SAXS curve of solution at room temperature.

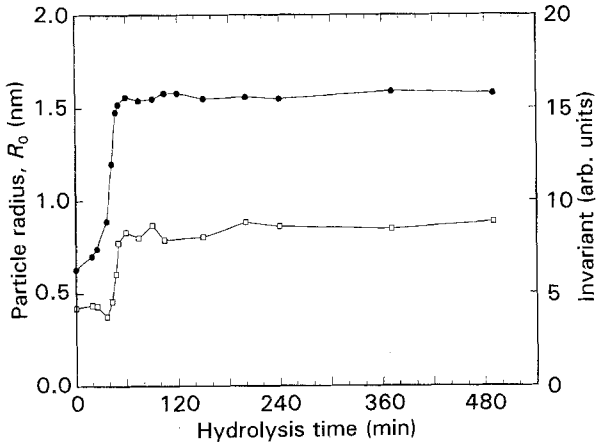

Figure 4 Variation of (●) radius, R_0, of particles and (□) invariant, Q, during hydrolysis.

position of the minimum of the intensity profile ($q_{min} \approx 2.5\ nm^{-1}$ or ln $q = -1.39$), in reasonable agreement with the value of 1.58 nm found by Guinier's law. The size stays constant, for ageing times up to 8 h. Neither the shape nor the intensity of the profile vary further, as illustrated in Fig. 4 which shows the time evolution of the invariant Q (see Equation 2). It is constant in Regime III. With the reasonable assumption that the average electronic density of the colloidal particles does not change, one can conclude that the total scattering volume, V, stays constant as, therefore, does the average number of scatterers in the solution, after the ageing temperature is reached.

Hence SAXS has showed us that colloids grow during the heating process up to a diameter of about 3 nm, then both their number and size remain constant and no larger particles are detected by the technique until precipitation occurs.

3.2.2. Local order study

Fig. 5 shows the evolution of the Fourier transforms of the EXAFS signal as the reaction proceeds from room temperature to ageing temperature ($T = 90$ °C). Three regimes are also observed, similar to the SAXS results. In Regime I, up to 55 °C, the Fourier transforms are comparable to that of the stock precursors: the structure of the species in solution does not change. Above 60 °C, structural modifications are observed in the Fourier transforms: Regime II is characterized by a continuous structural evolution from precursor to colloid. In Regime III, when the ageing temperature is reached, the shape of the Fourier transforms (Fig. 6) does not change significantly: the solution has reached an equilibrium state.

The Fourier transforms shown in Figs 5 and 6 are composed of three clearly resolved peaks in the range 0.10–0.24 nm for Peak A, 0.24–0.32 nm for Peak B and 0.34–0.39 nm for Peak C which can be assigned, to Ce–O, Ce–S and Ce–Ce distances, respectively. Peak B could not be fitted because no suitable model

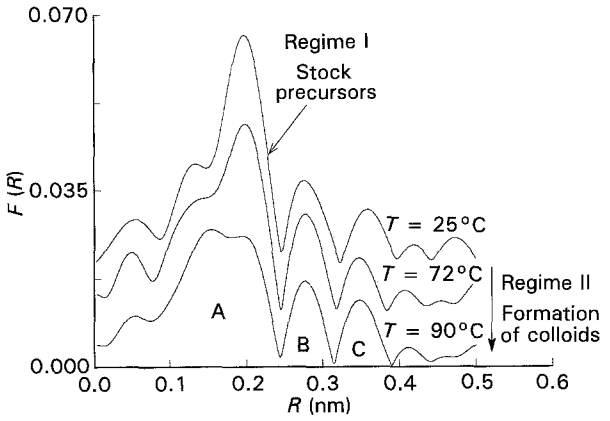

Figure 5 Change in the Fourier transforms of EXAFS of the solution between room temperature and 90 °C: stock solution, $T = 25$ °C, $t = 0$; thermohydrolysed sample, $T = 72$ °C, $t = 45$ min; thermohydrolysed sample, $T = 88$ °C, $t = 66$ min. The radial distribution functions for the stock solution and the first sample ($T = 72$ °C) are shifted on the y-axis by 0.02 and 0.01 units, respectively.

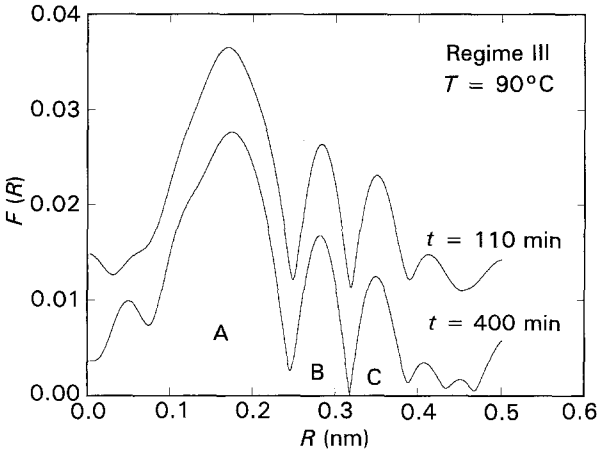

Figure 6 Fourier transforms of solutions aged for 110 and 400 min at 90 °C. The curves are shifted on the y-axis by 0.01 units.

compound of known structure was found to test the fitting parameters for a cerium–sulphur shell. Table I lists the fitting parameters for the cerium–oxygen shell of the Fourier transforms represented in Figs 5 and 6.

Peak A shows two resolved maxima. It is reasonable to assume that they correspond to two cerium–oxygen contributions. Consequently, this peak has been fitted with a two-shell procedure. The total number of oxygen atoms is constant for all samples with an average value of 8.0 ± 0.8 but the weight of the two contributions evolves from precursors to colloids during the first 2 h of hydrolysis. This evolution is better seen in Fig. 7 which summarizes the results obtained on the oxygen peak for the solutions before precipitation. The horizontal axis represents the length of time of hydrolysis before the sample is extracted from the reaction bath, whereas the vertical axis is the number of oxygen neighbours in each subshell. As the error in the determination of the neighbours number is estimated to be of the order of 10% –20%, when the ageing temperature is reached, the number of oxygen atoms is 6.0 ± 1.0 at 0.220 nm and 2.5 ± 0.5 at 0.241 nm.

According to the crystallographic data known for $Ce_2(OH)_2(SO_4)_3 \cdot 4H_2O$ [52] and $Ce_6O_4(OH)_4(SO_4)_6$ [53], the oxygen shell at 0.220 nm can be attributed to Ce–O distances in hydroxo-bridges. Consequently, we observe an increase of the number of hydroxo-bridges around the cerium atom from precursor to colloid. The Ce–O distance at 0.241 nm is related to the Ce–O bond with the oxygen atom of the sulphate ions and/or water which are located in a terminal position in the polyhedron of coordination (no bridging atoms).

Table II gives the fitting parameters for the cerium–cerium contribution in the stock solution and in the sol. This contribution has been fitted with a one shell procedure. The increase of the number of cerium neighbours and the decrease of Ce–Ce distance from precursor to colloid is also in line with the formation of a hydroxysulphate network via hydroxylation and condensation mechanisms.

Figs 8 and 9 show the fits in R space for the precursors and for the colloidal particles: (a) of the cerium–oxygen shell, (b) of the cerium–cerium shell. The characterization of the Ce–O and Ce–Ce shells in the precursor and colloids allows us to propose a di- or trimeric structure of the first and chain structure for the second ones, the cerium atoms being linked together by hydroxo-bridges.

3.2.3. pH measurements

pH measurements of the stock and thermohydrolysed solutions confirm that a deprotonation occurs during the forced hydrolysis as expected for such a reaction (see Fig. 10): the difference in proton concentration between the stock solution (0.38 M) and solutions (0.46 M) sampled when the ageing temperature is reached is almost + 0.08 M. Similar to the observations of SAXS and EXAFS, the system reaches an equilibrium state: at the end of the heating step, the proton concentration has levelled off.

TABLE I Parameters of the first coordination shell split in two subshells noted 1 and 2 for the Fourier transforms represented in Figs 5 and 6

Regime	T (°C)	Time (min)	N_1	R_1 (nm)	σ_1 (nm)	ΔE_1 (eV)	N_2	R_2 (nm)	σ_2 (nm)	ΔE_2 (eV)	N_{Total}
I	25	0	6.0	0.240 (2)	0.0094	7.3	2.0	0.221 (2)	0.0125	3.4	8.0
II	72	45	4.7	0.240 (2)	0.0094	6.8	3.1	0.219 (2)	0.0117	3.5	7.8
	90	66	3.7	0.240 (2)	0.0097	5.7	4.4	0.219 (2)	0.0119	3.5	8.1
III	90	110	2.9	0.241 (2)	0.0098	7.3	5.1	0.220 (2)	0.0126	3.6	8.0
	90	400	2.8	0.242 (2)	0.0086	5.3	5.7	0.221 (2)	0.0125	3.8	8.5

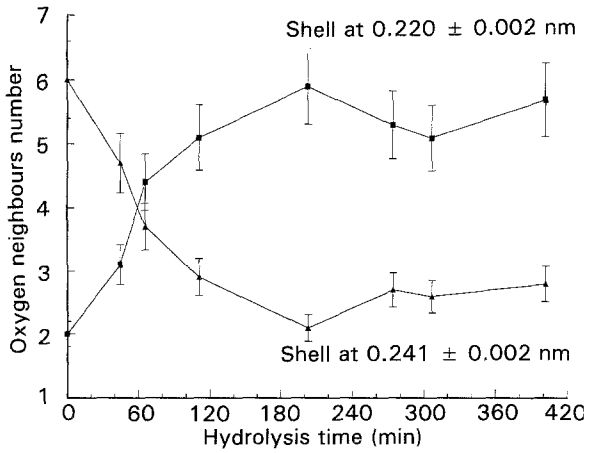

Figure 7 Variation of the oxygen contribution to the two shells of Peak A during hydrolysis.

TABLE II Parameters of the cerium shell for the precursors and colloids

Sample	N	R (nm)	σ (nm)	ΔE (eV)
Precursors in stock solution	1.2	0.370 (2)	0.0111	− 7.5
Colloids in sol	2.0	0.366 (2)	0.0124	− 6.5

3.3. Characterization of colloidal particles in solution

The following characterization of the size and shape of colloids and of the local order around the cerium atom, corresponds to solutions that have been thermohydrolysed for 120–130 min at 90 °C and have thus reached equilibrium (Regime III).

3.3.1. Size distribution of colloidal particles

The size distribution of the colloidal particles has been investigated by ultracentrifuge analysis. Fig. 11 shows the distribution of the sedimentation coefficient, S, of a colloidal dispersion. There is only one distribution centred around the value $S_0 = 8.85$ Svedbergs; this distribution function is characteristic of small particles with a polydispersity index (FWMH/$G(S)_{max}$) estimated to be of the order of 1.23.

In order to determine the molecular weight, M_{cp}, and/or the radius, R_{cp}, of the colloids, according to Equation 4, we need to know the partial specific volume of the particles, V_{ps}, and the density of the solution, ρ_0. At this point, if we assume that the particles are formed by condensation of the same molecular building blocks of molar weight M_m, we have a choice between three known species of cerium (IV) sulphate, i.e., $Ce(SO_4)_2 \cdot 4H_2O$ [54], $Ce_2(OH)_2(SO_4)_3 \cdot 4H_2O$ [52] and $Ce(OH)_2SO_4 \cdot nH_2O$ ($n = 0$, 1 and 2) [55]. The structure of the first two species is described in the literature, whereas the existence of the third one is only mentioned. Some pertinent data are collected in Table III.

For all monomeric species, the particle radii, R_{cp}, obtained from the ultracentrifuge measurements agree with the experimental radii determined by SAXS, provided the particle density lies in the range

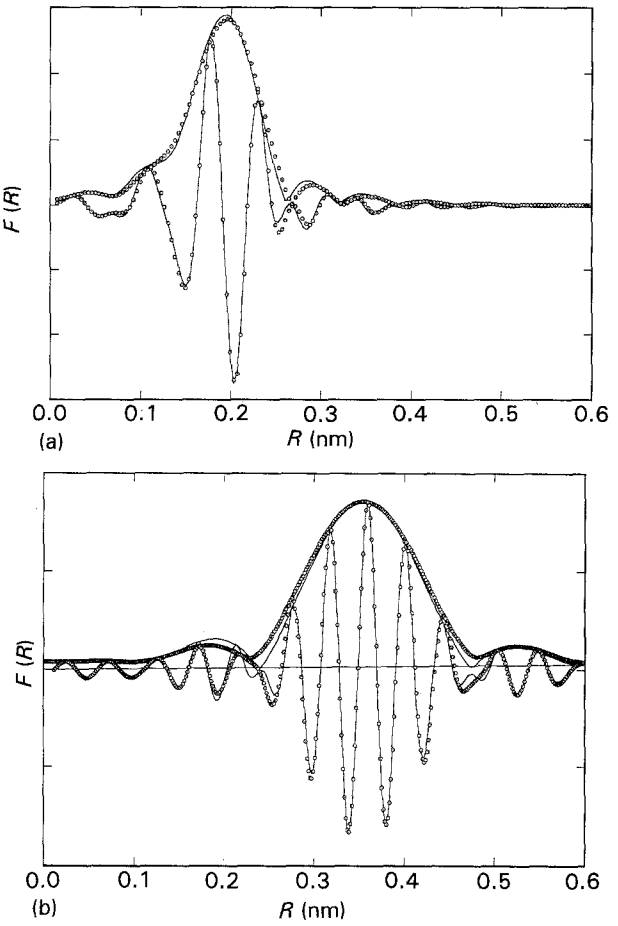

Figure 8 (a) (——) Fit of the Fourier filtered Peak A (○); (b) (——) fit of the Fourier filtered Peak C (○) for the precursors.

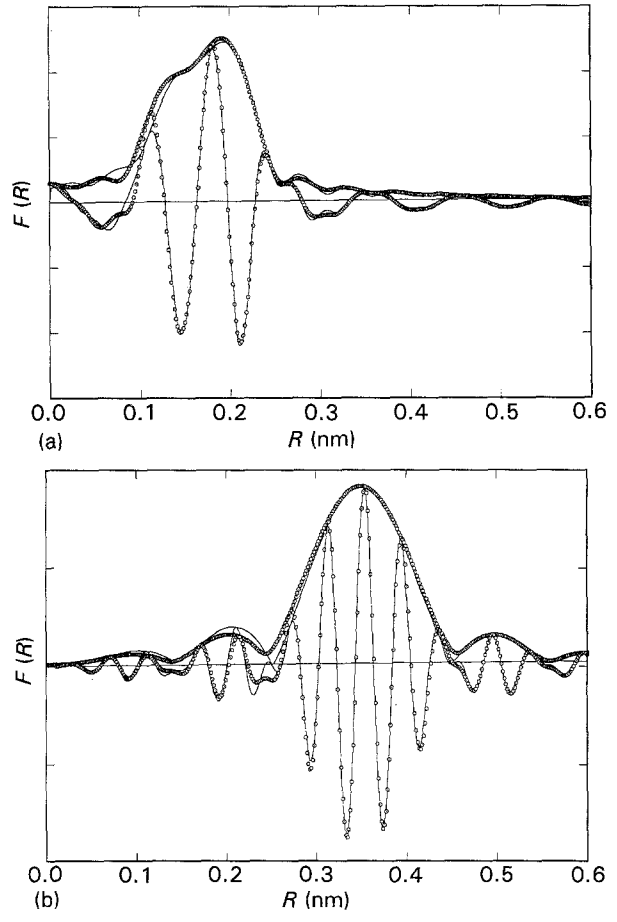

Figure 9 (a) (——) Fit of the Fourier filtered Peak A (○); (b) (——) fit of the Fourier filtered Peak C (○) for the colloidal particles.

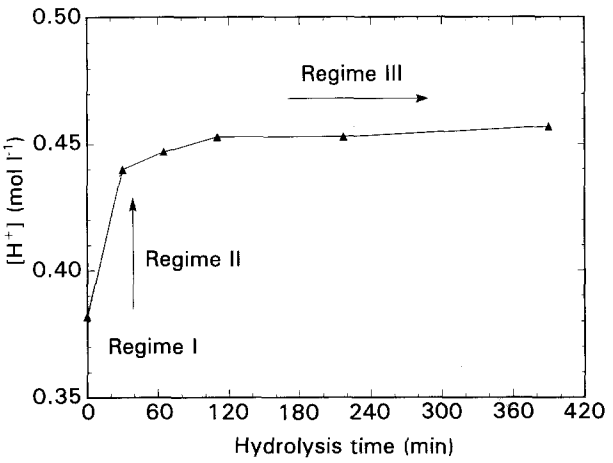

Figure 10 Variation of the proton concentration during hydrolysis.

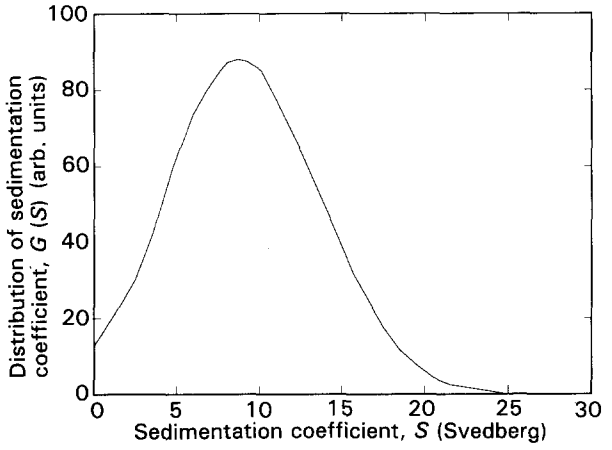

Figure 11 Distribution of sedimentation coefficient, S, measured on a colloidal solution (hydrolysis at 90 °C for 130 min)

2.7–4.3 g cm^{-3}. However, it does not agree for the dimeric precursor $Ce_2(OH)_2(SO_4)_3 \cdot 4H_2O$ for a reasonable value of the density. Consequently, a mechanism of condensation of precursors to form colloids could involve monomeric species only. It is then possible to obtain an order of magnitude of the degree of condensation, X, as $(M_{cp})/(M_m)$. It is found to be between 50 and 70 elementary monomers for a radius of 1.5 nm: with this model, the structure of the colloids is therefore more disordered than that of the oxide CeO_2 which would contain around 500 atoms of cerium in the same volume.

3.3.2. Repartition of species in the colloidal solution

After ultracentrifugation at 50 000 r.p.m. for 15 h of the same sample, i.e. thermohydrolysed for 120 min at 90 °C, according to the measured sedimentation coefficient, all colloids should be in the lower half of the sample cell. Hence the supernatant solution in the upper half contains only the solvent with some ceric species, but no colloids. The Ce(IV) concentration there, measured by a standard potentiometric method, is found to be 0.015 M. Because the ceric concentration in the stock solution was 0.1 M, the colloidal solution is therefore 0.085 M in Ce(IV). Hence it is concluded that, at equilibrium, $\approx 85\%$ of the ceric species in a thermohydrolysed sample are colloids with a radius of 1.5 nm; the rest is made of smaller species.

In order to characterize the Ce(IV) species not included in the colloids, the EXAFS spectrum of the supernatant solution has been compared to that of the stock solution. As shown in Fig. 12a and b, the Ce–O and Ce–Ce contributions to the Fourier transforms are almost identical whereas the amplitude of the Ce–S peak is more intense after centrifugation, indicating a different sulphur environment. The species characterized by EXAFS in the supernatant solution have, to a first approximation, the same oxygen surroundings around the cerium than that encountered in the stock solution. The increase of the amplitude of the Ce–S peak can be explained by a different sulphate environment in both solutions: the supplementary sulphate ions are not in the coordination sphere of the cerium but in the solvation sphere around the species. We conclude that the 15% of the Ce(IV) species are similar to the precursors.

The colloid-rich solution in the lower half of the ultracentrifuge cell has also been characterized by EXAFS. The Fourier transform in Fig. 12c is rigorously identical to that of the original sample before centrifugation (Fig. 12d). One can assume that the EXAFS signal of the thermohydrolysed solution is dominated by the contribution of the colloids and that the signal of the precursors is negligible.

At this point of our EXAFS analysis of the colloids, we must state precisely that the description of the first coordination shell around the cerium in terms of two shells (6.0 ± 1.0 oxygen atoms at 0.220 nm and 2.5 ± 0.5 other ones at 0.241 nm) is a reasonable approximation, but it is not rigorously exact. Indeed, the shell at 0.220 nm is split in reality into two subshells: 4.0 ± 0.2 oxygen atoms at 0.222 nm and 2.0 ± 1.0 other ones at 0.212 nm. Table IV compares the

TABLE III Fitting parameters for the cerium–cerium contribution in stock solution and sol

Possible monomers	Monomers molar weight, M_m	Colloidal particles density, ρ_{cp} (g cm^{-3})	Colloidal particles radius, R_{cp} (nm)	Colloidal particles molar weight, M_{cp}	Condensation degree $X = M_{cp}/M_m$
$Ce(OH)_2SO_4$	270	4.29	1.10	14 575	54
$Ce(OH)_2SO_4 \cdot H_2O$	288	3.55	1.26	17 760	62
$Ce(OH)_2SO_4 \cdot 2H_2O$	306	3.12	1.38	20 592	67
$Ce(SO_4)_2$	332	2.69	1.55	25 094	75
$Ce_2(OH)_2(SO_4)_3 \cdot 4H_2O$	674	1.47	2.98	97 609	145

TABLE IV Parameters of the first coordination shell in the case of a two-shell procedure and three-shell procedure for the Fourier transforms representated in Fig. 12d

	Shell number, i	N_i	R_i (nm)	σ_i (nm)	ΔE_i (eV)	N_{Total}
Two-shell procedure	1	2.9	0.241 (2)	0.0098	7.3	8.0
	2	5.1	0.220 (2)	0.0126	3.6	
Three-shell procedure	1	3.1	0.240 (2)	0.0091	7.3	8.1
	2	4.0	0.223 (2)	0.0123	3.9	
	3	1.0	0.212 (2)	0.0077	1.3	

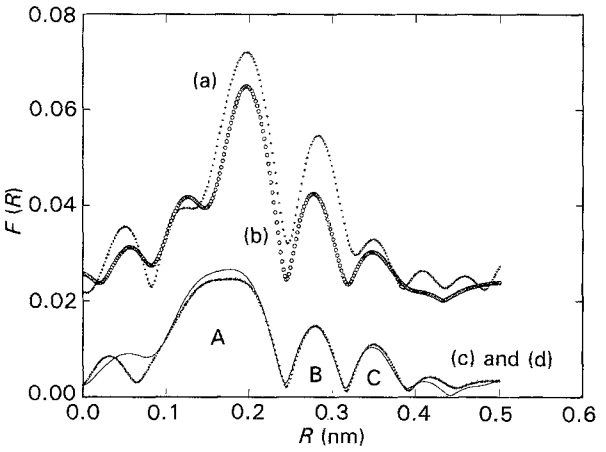

Figure 12 Fourier transforms: (a) of the supernatant solution (+) after preparative centrifugation of thermohydrolysed solution; (b) of the stock solution of the thermohydrolysis (○); (c) of the concentrated solution (+) after preparative centrifugation of thermohydrolysed solution, and (d) of the thermohydrolysed solution (——) before centrifugation. Curves (a) and (b) are shifted vertically by 0.02 units.

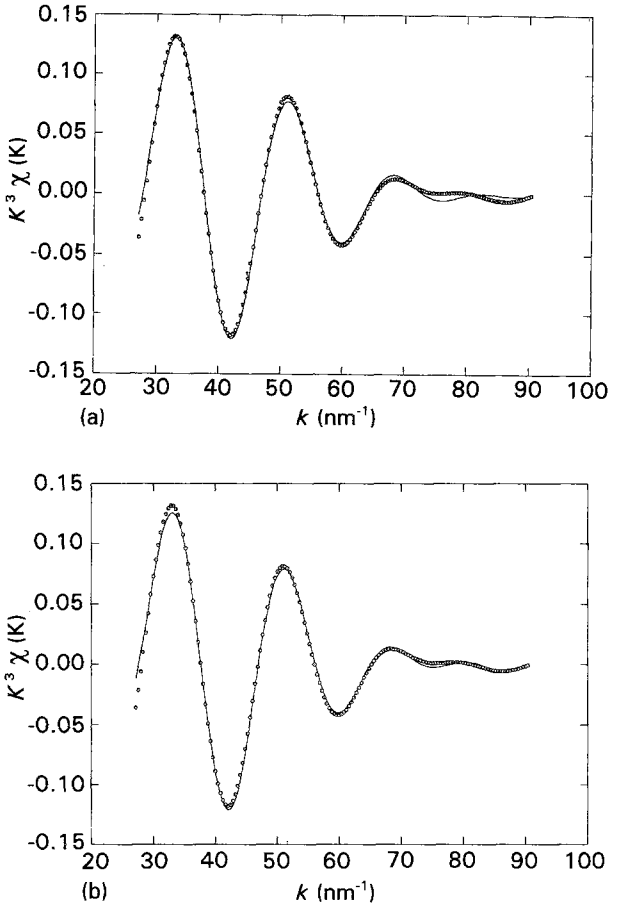

Figure 13 (——) Fit of the Fourier filtered Peak A (○) of Fig. 12d; (a) fit with a two shell procedure; (b) with a three-shell procedure.

fitting parameters for the cerium–oxygen contribution of the Fourier transform in Fig. 12d in the case of a two-shell procedure and of a three-shell one.

Fig. 13a and b, which represent the fitting and experimental curves in k space, illustrate this comparison of procedures. The beat located at 70–90 nm^{-1} which is produced by the sum of sine waves (each sine wave being related to one sub-shell) at different frequencies [43], is better simulated with the three-shell procedure than with the two-shell one. Note that this short cerium–oxygen distance (0.212 nm) is also found in the solid related to the colloidal particles extracted from the solution, which will be discussed in Part III [29].

From the comparison with model compounds, it is clear that the Ce–O distance at 0.222 nm is related to the formation of hydroxo-bridges between two cerium atoms, whereas the oxygen atoms at 0.241 nm are attributed to terminal groups (sulphate ions and/or water). Thus, some polymerization of the precursors has taken place. The short cerium–oxygen bond at 0.212 nm is often encountered in cerium (IV) alkoxide [56] or arylsiloxide [57] complexes: it corresponds in these cases to terminal bulky groups. Such a bond length also exists in anhydrous cerium (IV) disulphate $Ce(SO_4)_2$ [58]. Namely, in this structure, each sulphate group is bonded to four cerium atoms with Ce–O distances ranging from 0.207–0.238 nm; the four oxygen atoms of the sulphate are bridging atoms. Thus we can relate the short Ce–O distance encountered in the colloidal particles to the formation of chemical bonds between sulphate groups and cerium atoms.

3.3.3. TEM observations

We have also attempted to characterize the colloidal solutions by HRTEM. Imaging of the dried film shows a continuous transformation upon irradiation, from a featureless background to fringe systems with domains of about 3.0 nm. No larger particles are visible. Simultaneous microanalysis shows a loss of sulphur and oxygen, whereas the electron diffraction pattern, characterized initially by two broad rings, transforms into the reflection peaks of crystalline CeO_2.

This evolution shows that some sulphate ions were indeed in the coordination shell of the cerium atom in the colloidal particles before irradiation and gives credit to the previous attribution of Peak **B** in the

EXAFS Fourier transform to a sulphur shell signal (Figs 5 and 6). As will be reported in Part III [29], this is also confirmed by infrared data on aggregated dried colloids extracted from the solution which show the formation of a hydroxysulphate network.

If one assumes that the domains appearing after irradiation reflect the original colloids, TEM also confirms the previous conclusions that the only particles in the solution before precipitation are roughly circular colloids of about 3.0 nm.

4. Discussion

At this point, it is possible to give a structural description of the chemical species characterized during the three regimes of the thermohydrolysis, consistent with the previous data.

4.1. Regime I: $T = 25$–$55\,^{\circ}C$

In Regime I, the solutions hydrolysed between 25 and 55 °C contain the same chemical species as the stock solutions, i.e. precursors.

The absence of scattering at small angles indicates that the precursors are small species (size < 0.5 nm) and therefore are probably not bigger than dimers or trimers. EXAFS provides complementary information on the structure of the precursors: two hydroxo-bridges (d(Ce–O) = 0.220 nm) bonding cerium atoms (d(Ce–Ce) = 0.370 nm) are found in the precursors and the polyhedron of coordination around the cerium is completed by six oxygen atoms (d(Ce–O) = 0.241 nm). However, it is not possible with these data only to identify the exact chemical nature of the precursors.

A dimeric structure compatible with the results obtained so far is represented in Fig. 14.

Amongst the possible models, this dimeric species is also compatible with the high proton concentration measured in the stock solution (0.38 M). Indeed, it is unambiguously formed of two OH^- bridged ligands and results from a spontaneous hydrolysis and dimerization of the complex produced by the dissolution of $Ce(SO_4)_2$ in sulphuric acid. In aqueous solution sulphuric acid generates disulphate and sulphate ions according to the following reactions

$$H_2SO_4 + H_2O \rightleftharpoons HSO_4^- + H_3O^+ \ (E_1)$$

$$HSO_4^- + H_2O \rightleftharpoons SO_4^{2-} + H_3O^+ \ (E_2)$$

The first dissociation (E_1) is generally considered as complete, whereas the second dissociation (E_2) prevails only at very low acid concentration [59]. Taking into account the value of the equilibrium constant of (E_2) ($KE_2 = 0.01055$ at 25 °C [59]) and remembering that the initial solution was 0.25 M in sulphuric acid, the resulting acidity from both (E_1) and (E_2) is equal to 0.26 M. The increase in the acidity of solution (+ 0.12 M) with respect to the acidity of sulphuric acid is due to a spontaneous hydrolysis which (i) releases protons in the solution and (ii) generates hydroxo ligands in the first coordination cerium shell. The latter feature is important because the presence of at least one such ligand is a necessary condition for condensation reactions to occur [12, 13].

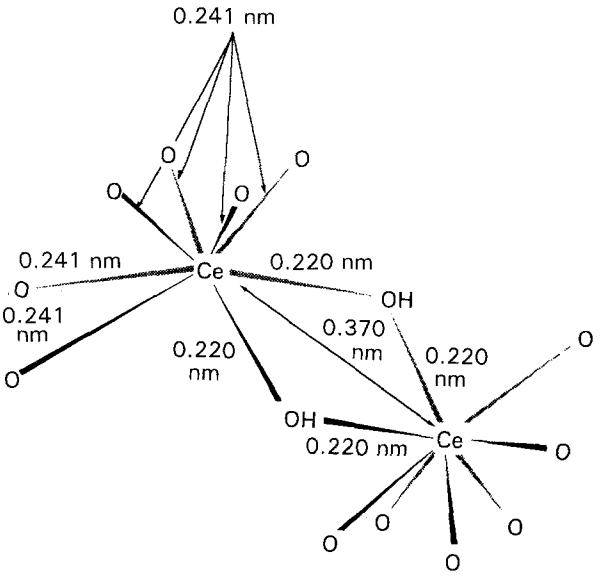

Figure 14 Proposed dimeric structure for the precursors.

We can also conclude that condensation is inhibited after the first step, leading to the formation of dimeric precursors, because no larger oligomeric species have been detected by SAXS.

4.2. Regime II: $T = 60$–$90\,^{\circ}C$

In Regime II, the thermohydrolysed solutions contain new chemical species, the colloids.

SAXS shows clearly the growth of particles, with radius R_0 increasing from 0.5 nm to 1.2 nm. This growth also involves a continuous structural evolution around the cerium characterized by EXAFS. The relevant transformations are evidenced by an increase of both the number of hydroxo bridges around the cerium and the number of cerium neighbours. Simultaneously, the acidity of solution increases to + 0.08 M.

These results can be interpreted as follows. Forced hydrolysis leads to a further deprotonation of the precursors; new species are formed which condense rapidly through olation mechanisms to produce colloids.

4.3. Regime III: $T = 90\,^{\circ}C$

After 1 h thermal treatment, and until precipitation occurs, the system is characterized by a constant number of colloidal scattering particles with constant shape and size and no change of the local order around cerium. From the point of view of the SAXS and EXAFS techniques, the solution has reached an equilibrium state.

The structure of the colloidal particles determined by EXAFS is in agreement with a chain structure where one cerium atom is linked to two other ones (d(Ce–Ce) = 0.366 nm) by four hydroxo bridges (d(Ce–O) = 0.222 nm). The elementary block deduced from the EXAFS results is shown in Fig. 15a. As for

the precursors, the type of bonds in which the four oxygen atoms are involved (those at 0.241 nm and those at 0.212 nm) cannot be identified precisely. All that we know from the EXAFS and TEM characterizations is that some sulphur atoms are included in the first coordination shell around the cerium. They are likely to belong to bridging sulphate groups but their number is not known.

SAXS and ultracentrifuge measurements show that this structure extends over distances of the order of 3 nm (see Fig. 15b). Furthermore, the colloids formed are close to monodisperse, spherical particles. In view of the chemical structure of the dimer proposed as precursor, the colloidal particles will contain chains of composition $(Ce(OH)_2)_n^{2n+}$. Fig. 15c shows a possible 3-d structure of the colloids, largely inspired by a description of infinite chains of composition $(M(OH)_2)_n^{2n+}$ found in the literature for the $M(OH)_2(SO_4)$ structure where M = Hf, Zr, Th, U [60–63]. The bulk of the particles is composed of layers of portions of chains linked together by sulphate anions. This arrangement is compatible with a less compact structure than that of the oxide CeO_2, as observed by ultracentrifuge analysis.

Finally, it was found that, at the equilibrium state characteristic of this Regime III, only 85% of the total Ce(IV) are in the form of colloidal particles. It can be concluded that forced hydrolysis which generates colloids by deprotonation and condensation of the initial dimeric precursors is not a complete reaction.

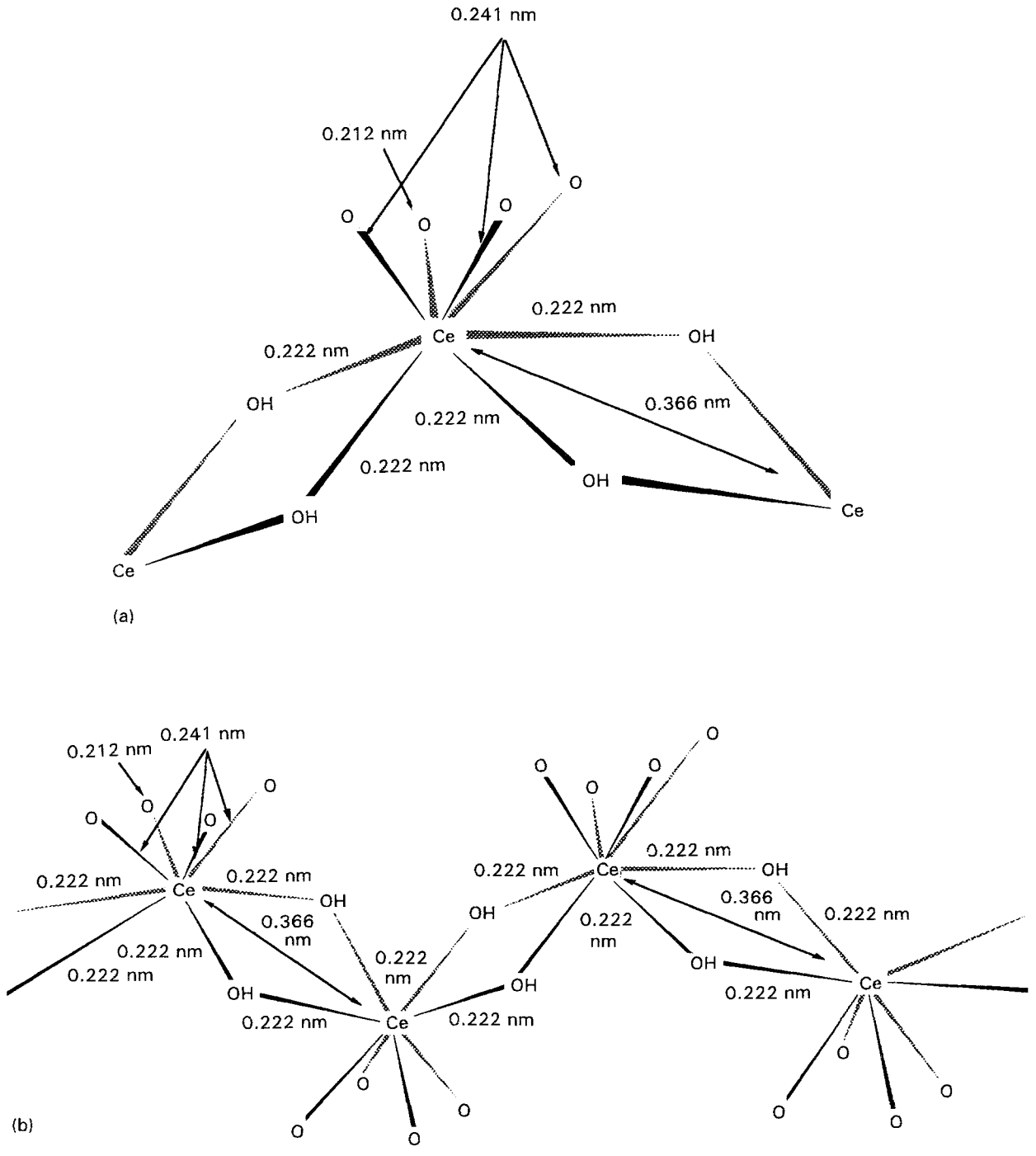

Figure 15 (a) Elementary block characterized by EXAFS; (b) 3.0 nm length of chains deduced from SAXS results; (c) Possible isotropic structure of colloids in solution.

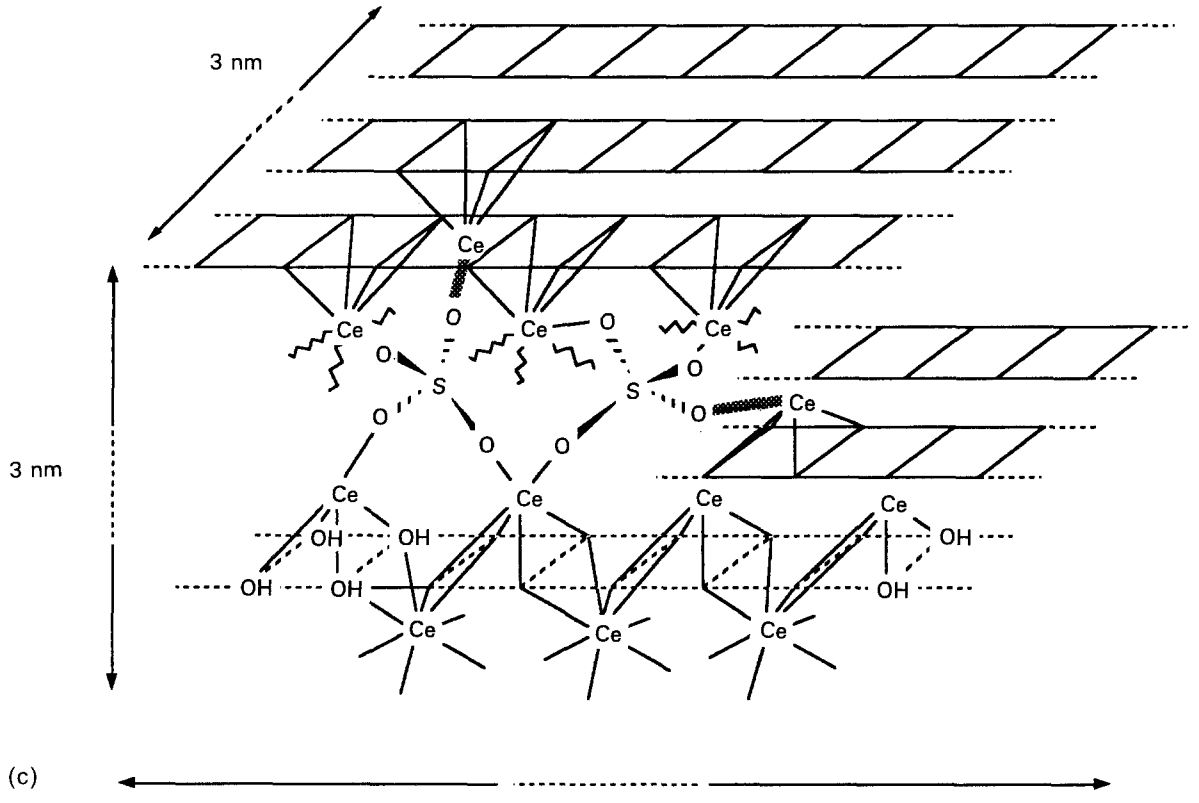

Figure 15 continued.

The remaining 15% are smaller particles which can be isolated by ultracentrifugation. In solution, they cannot be detected directly by any of the techniques used here, because their presence is hidden by the more numerous bigger colloids. However, they are the leading components for producing the final solid $CeOSO_4 \cdot H_2O$, as will be discussed in Part III, together with a detailed characterization of the particles.

5. Conclusion

This paper gives a full description of the different steps of the forced hydrolysis of solutions of Ce(IV) sulphate [25] that lead to uniform colloidal particles of controlled morphology. It uses the structural techniques of EXAFS and SAXS to describe the solution at different length scales, from 0.1–10 nm, complemented by pH and centrifugation measurements.

Two stages have been characterized in solution.

1. In the first stage the solution contains only dimeric precursors of composition $Ce_2(OH)_2(O)_{12}$. The twelve oxygen atoms belong to sulphate ions and/or water. At this point different chemical models are possible. To choose between them, it will be necessary to use the theoretical model of partial charges developed by Livage *et al.* [12, 13] which can predict the reactivity of chemical species, and consequently the stability, in aqueous solution. This will be discussed in Part II [28].

After the initial stage, colloids appear when the temperature rises above 60 °C. The solution contains then colloidal particles in increasing number and size, together with the precursors.

2. When the ageing temperature is reached (90 °C), the second stage is obtained. It is characterized by colloids (85%) and smaller particles (15%). The colloids are relatively monodisperse spherical particles of 1.5 nm radius. They are formed at higher temperature by an inorganic polymerization involving deprotonation and condensation mechanisms starting from dimers formed at room temperature. A solid hydroxysulphate network is formed. The EXAFS study is in agreement with a chain structure of composition $(Ce(OH)_2)_n^{2n+}$ where the cerium atoms (d(Ce–Ce) = 0.366 nm) are linked together via hydroxo-bridges (d(Ce–OH) = 0.222 nm). The formation of these hydroxo-bridges is related to hydroxylation and condensation (by olation) mechanisms, as will be explained in Part II [28].

In Part III, we will discuss the precipitation mechanisms leading to the final $CeOSO_4 \cdot H_2O$ solid [29].

Acknowledgements

We thank Rhône-Poulenc Chemicals for partial financial support. One of us (V.B.) thanks the engineers and technical staff of the Centre de Recherche Rhône-Poulenc d'Aubervilliers, for the use of laboratory facilities and technical assistance. The participation of J. Eberle and J. Lemerle in the ultracentrifuge study, and of J. L. Mansot in the TEM investigation, is acknowledged.

References

1. L. L. HENCH and D. R. ULRICH (Eds) "Ultrastructure Processing of Ceramics, Glasses and Composites" (Wiley-Interscience, New-York, 1984).
2. E. MATIJEVIC, *Pure Appl. Chem.* **60** (1988) 1479.
3. Ph. TAILHADES, P. MOLLARD, A. ROUSSET and M. GOUGEON, *IEEE Trans. Magnetics* **26** (1990) 1822.

4. E. MATIJEVIC, *Progr. Colloid. Polym. Sci.* **61** (1976) 24.
5. *Idem, Pure Appl. Chem.* **52** (1980) 1193.
6. *Idem, Acc. Chem. Res.* **14** (1981) 22.
7. *Idem, Ann. Rev. Mater. Sci.* **15** (1985) 483.
8. *Idem, Langmuir* **2** (1986) 12.
9. T. SUGIMOTO, *Adv. Colloid Interface Sci.* **28** (1987) 65.
10. *Idem, Mater. Res. Soc. Bull.* **14** (1989) 23.
11. M. HARUTA and B. DELMON, *J. Chim. Phys.* **83** (1986) 859.
12. J. LIVAGE, M. HENRY and C. SANCHEZ, *Pure Solid State Chem.* **18** (1988) 259.
13. J. LIVAGE, M. HENRY, J. P. JOLIVET and C. SANCHEZ, *Mater. Res. Soc. Bull.* **14** (1989) 18.
14. R. DEMCHAK and E. MATIJEVIC, *J. Colloid. Interface. Sci.* **31** (1969) 257.
15. E. MATIJEVIC and R. S. SAPIESZKO, *ibid.* **50** (1975) 567.
16. R. S. SAPIESZKO, R. C. PATEL and E. MATIJEVIC, *J. Phys. Chem.* **81** (1977) 1061.
17. E. MATIJEVIC and P. SCHEINER, *J. Colloid Interface. Sci.* **63** (1978) 509.
18. E. MATIJEVIC, M. BUDNIK and L. MEITES, *ibid.* **61** (1977) 302.
19. W. B. SCOTT and E. MATIJEVIC, *ibid.* **66** (1978) 447.
20. H. SASAKI, E. MATIJEVIC and E. BAROUCH, *ibid.* **76** (1980) 319.
21. N. B. MILIC and E. MATIJEVIC, *ibid.* **85** (1982) 306.
22. S. HAMADA, K. BANDO and Y. KUDO, *J. Chem. Soc. Jpn* **6** (1984) 1068.
23. D. H. BUSS, G. SCHAUMBERG and O. GLEMSER, *Angew. Chem.* **97** (1985) 1050.
24. M. A. BLESA, A. J. G. MAROTO, S. I. PASSAGGIO, N. E. FIGLIOLIA and G. RIGOTTI, *J. Mater. Sci.* **20** (1985) 4601.
25. W. P. HSU, L. RONNQUIST and E. MATIJEVIC, *Langmuir* **4** (1988) 31.
26. M. CASTELLANO and E. MATIJEVIC, *Chem. Mater.* **1** (1989) 78.
27. K. YURA, K. C. FREDRIKSON and E. MATIJEVIC, *Colloid Surf.* **50** (1990) 281.
28. V. BRIOIS, C. E. WILLIAMS, H. DEXPERT, M. HENRY J. P. JOLIVET, F. DENEUVE and C. MAGNIER, in preparation.
29. V. BRIOIS, C. E. WILLIAMS, H. DEXPERT, F. VILLAIN, M. VERDAGUER, A. POURPOINT, F. DENEUVE and C. MAGNIER, in preparation.
30. A. H. KUNZ, *Anal. Chem.* **53** (1931) 98.
31. E. WADSWORTH, F. R. DUKE and C. A. GOETZ, *Anal. Chem.* **12** (1957) 1824.
32. J. M. DUBUISSON, J. M. DAUVERGNE, C. DEPAUTEX, P. VACHETTE and C. E. WILLIAMS, *Nucl. Instrum. Meth. Phys. Res.* **A246** (1986) 636.
33. A. GUINIER and G. FOURNET, "Small Angle Scattering of X-rays" (Wiley, New York, 1955).
34. O. GLATTER, *Acta Phys. Aust.* **36** (1972) 307.
35. O. GLATTER and O. KRATKY (Eds) "Small Angle X-Ray Scattering" (Academic Press, London, 1982).
36. Ph. SAINCTAVIT, J. PETIAU, A. MANCEAU, R. RIVALLANT, M. BELAKHOVSKY and G. RENAUD, *Nucl. Instrum. Meth. Phys. Res.* **A273** (1988) 423.
37. P. LAGARDE, M. LEMONNIER and H. DEXPERT, *Physica B* **158** (1989) 337.
38. C. PRIETO, P. LAGARDE, H. DEXPERT, V. BRIOIS, F. VILLAIN and M. VERDAGUER, *Meas. Sci. Technol.* **3** (1992) 325.
39. D. E. SAYERS, F. W. LYTLE and E. A. STERN, *Adv. X-Ray Anal.* **13** (1970) 248.
40. D. E. SAYERS, E. A. STERN and F. W. LYTLE, *Phys. Rev. Lett.* **27** (1971) 1204.
41. F. W. LYTLE, D. E. SAYERS and E. A. STERN, *Phys. Rev. B* **11** (1975) 4825.
42. E. A. STERN, D. E. SAYERS and F. W. LYTLE, *ibid.* **11** (1975) 4836.
43. B. K. TEO, "Inorganic Chemistry Concepts" Vol. 9, "EXAFS: Basic Principles and Data Analysis" (Springer, Berlin, 1986).
44. A. G. Mc KALE, B. W. VEAL, A. P. PAULIKAS, S. K. CHAN and G. S. KNAPP, *J. Am. Chem. Soc.* **110** (1988) 3763.
45. F. TAULELLE, private communication (1991).
46. V. BRIOIS, J. LEMERLE and J. EBERLE, in preparation.
47. T. SVEDBERG and K. O. PEDERSEN, "The Ultracentrifuge" (Clarendon Press, Oxford, London, 1940).
48. G. CHAMPETIER, in "Chimie Macromoléculaire", Vol II (Hermann, Paris, 1972) Ch. V.
49. L. T. BUGAENKO and H. KUAN-LIN, *Russ. J. Inorg. Chem.* **8** (1963) 1299.
50. T. N. BONDAREVA, V. F. BARKOVSKII and T. V. VELIKANOVA, *ibid.* **10** (1965) 67.
51. L. V. TRUBACHEVA and N. I. PECHUROVA, *ibid.* **26** (1981) 1745.
52. O. LINDGREN, *Acta Chem. Scand.* **A31** (1977) 163.
53. G. LUNDGREN, *Arkiv Kemi* **10** (1956) 183.
54. O. LINDGREN, *Acta Chem. Scand.* **A31** (1977) 453.
55. G. V. TROFIMOV and V. I. BELOKOSKOV, *Russ. J. Inorg. Chem.* **13** (1968) 135.
56. W. J. EVANS, T. J. DEMING, J. M. OLOFSON and J. W. ZILLER, *Inorg. Chem.* **28** (1989) 4027.
57. P. S. GRADEFF, K. YUNLU, A. GLEIZES and J. GALY, *Polyhedron* **8** (1989) 1001.
58. D. L. ROGACHEV, M. A. PORAI-KOSHITS, V. Ya. KUZNETSOV and L. M. DIKAREVA, *J. Struct. Chem.* **15** (1974) 397.
59. K. S. PITZER, R. N. ROY and L. F. SILVESTER, *J. Am. Chem. Soc.* **99** (1977) 4930.
60. M. HANSSON, *Acta Chem. Scand.* **27** (1973) 2455.
61. M. EL BRAHIMI, J. DURAND and L. COT, *Eur. J. Solid State Inorg. Chem.* **25** (1988) 185.
62. G. LUNDGREN, *Arkiv Kemi* **2** (1950) 535.
63. *Idem, ibid.* **4** (1952) 421.

Received 30 July 1992
and accepted 3 February 1993